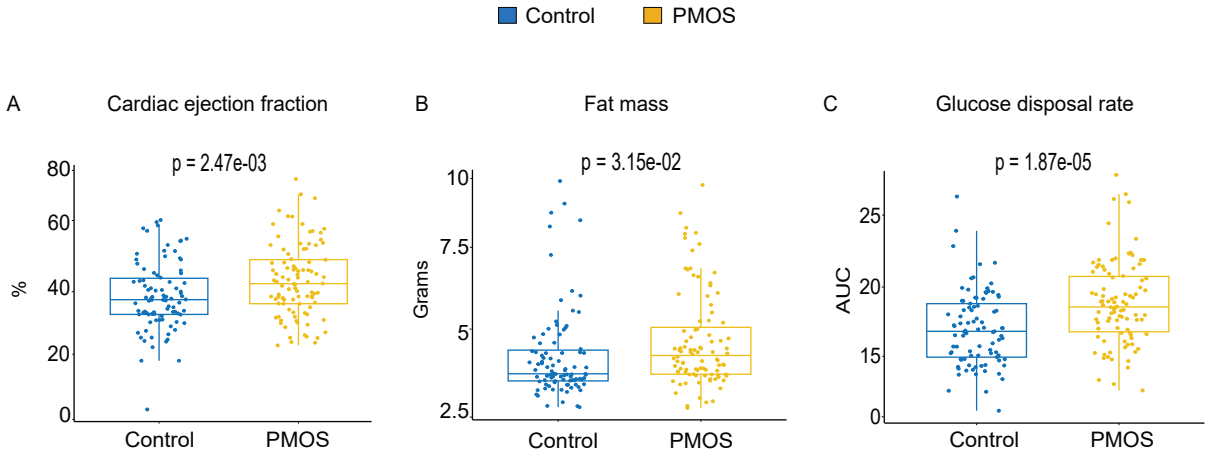
Control
PMOS
A
Cardiac ejection fraction
p = 2.47e-03
%
80
60
40
20
0
Control
PMOS
B
Fat mass
p = 3.15e-02
Grams
10
7.5
5
2.5
Control
PMOS
C
Glucose disposal rate
p = 1.87e-05
AUC
25
20
15
0
Control
PMOS

A

PMOS DEGs in adipose vs ovary

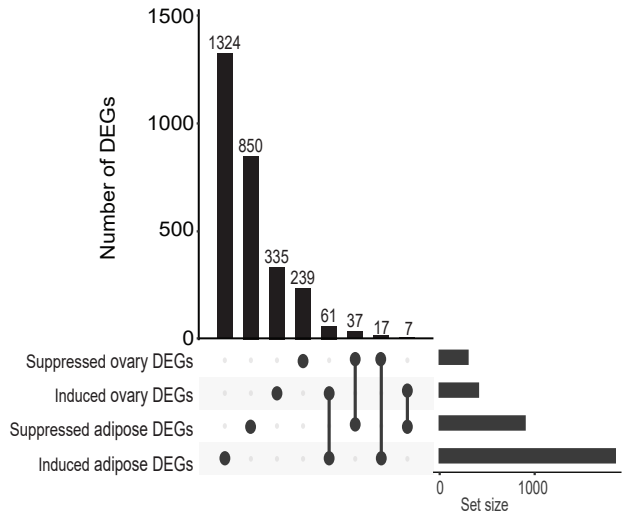

B

Top adipose PMOS enrichments

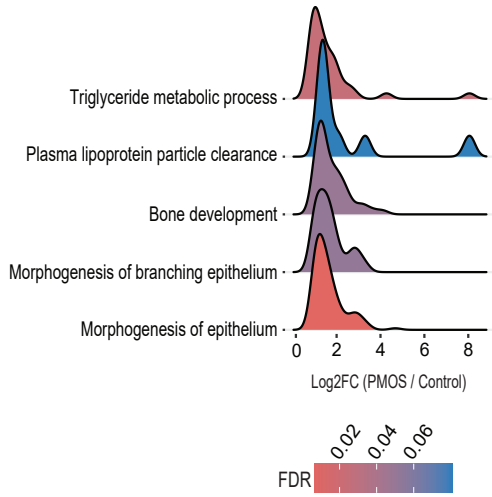

C

Intersection of human and mouse PMOS DEGs

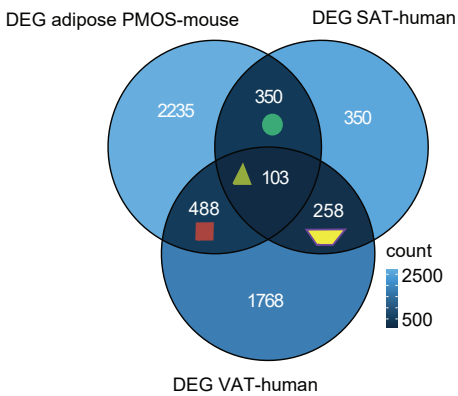

D

Pathways related to mouse-human PMOS intersection

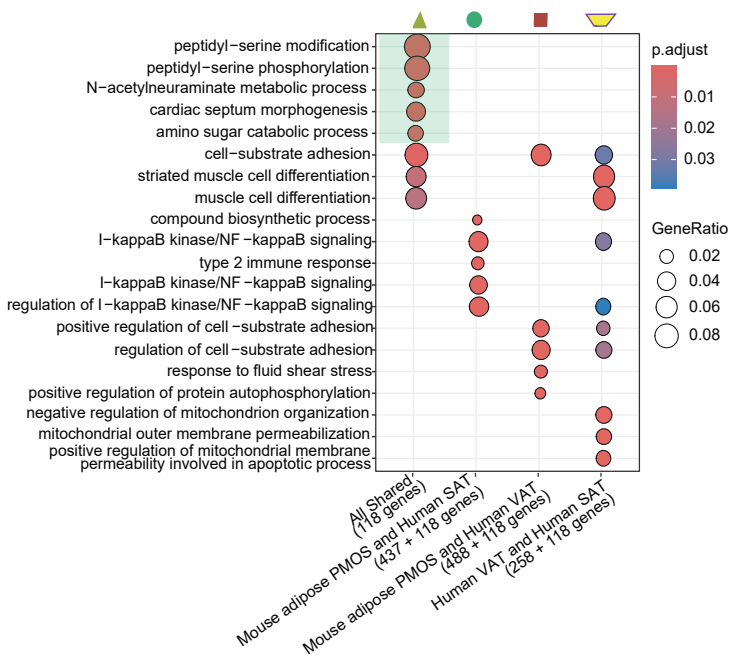

A

Conservation of adipose DEGs

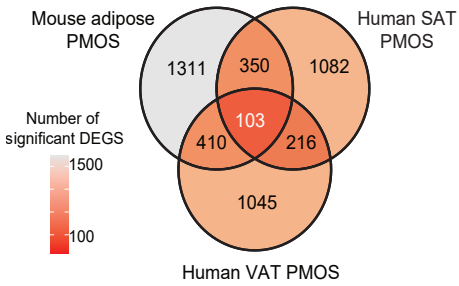

B

Single-cell localization of core conserved PMOS DEGS

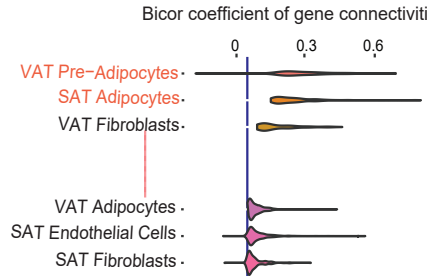

C

Colocalization with PMOS and T2D in SAT adipocytes

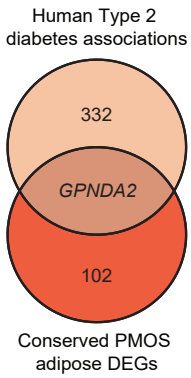

D

GNPDA2 gene network in VAT pre-adipocytes

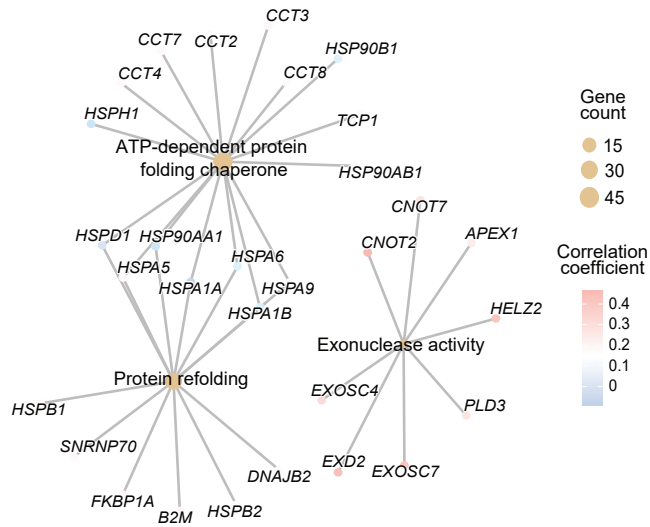

E

Colocalization with PMOS and CVD VAT pre-adipocytes

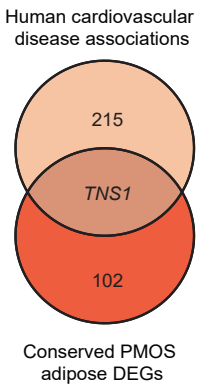

F

TNS1 gene network in mature SAT adipocytes

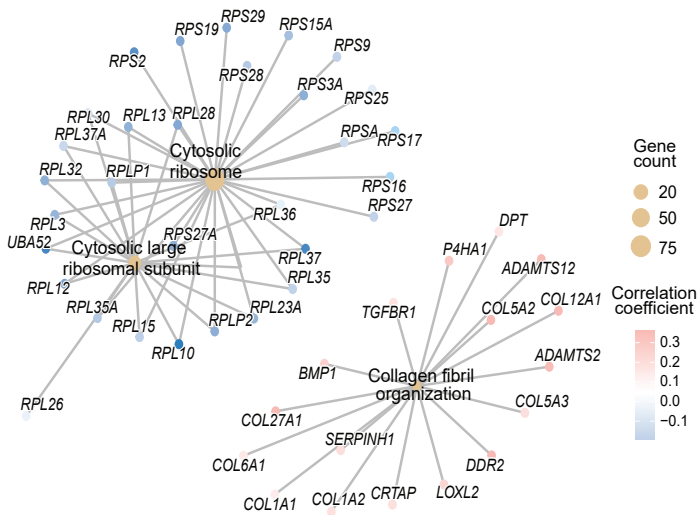

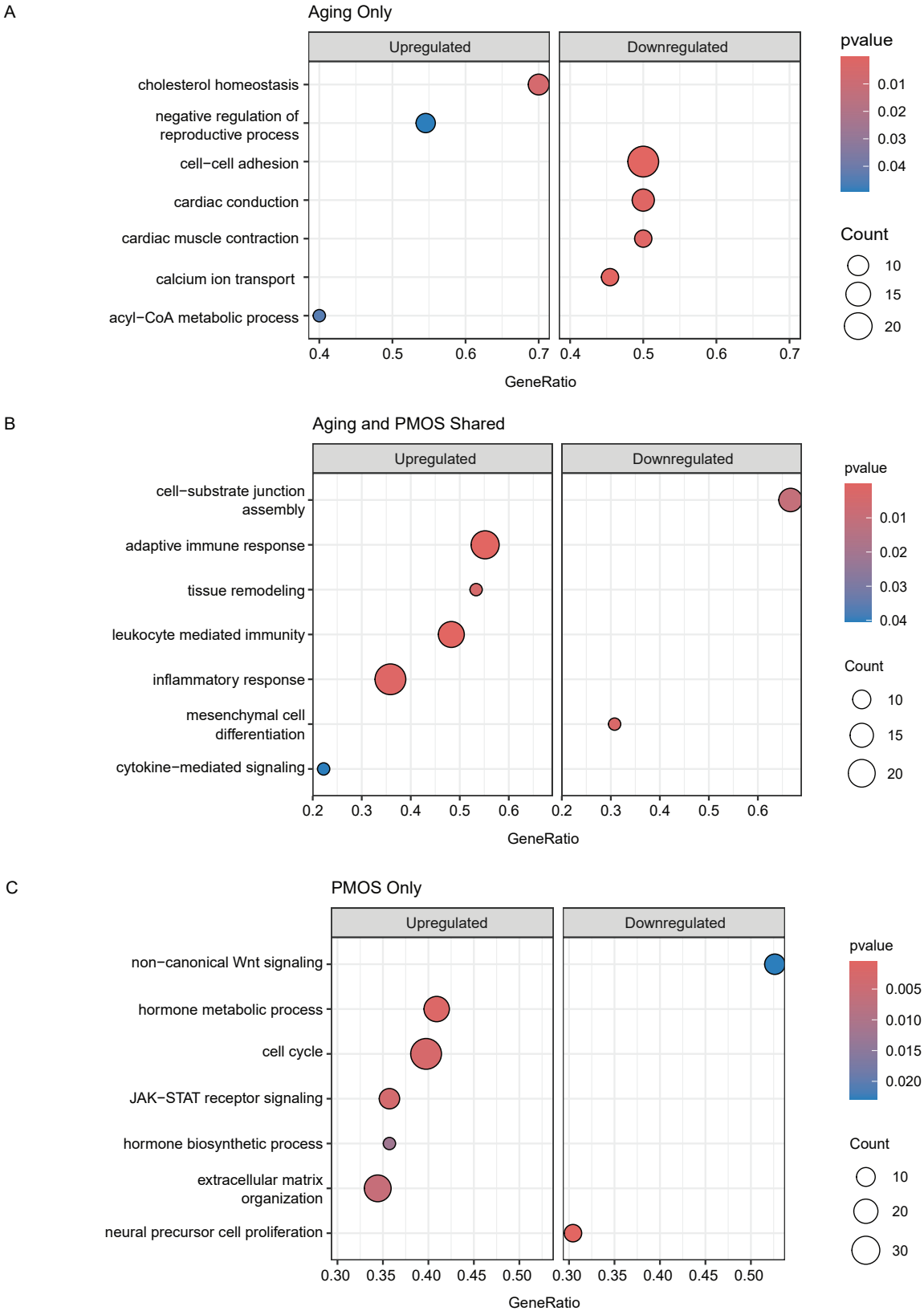
A
Aging Only
Upregulated
Downregulated
cholesterol homeostasis
negative regulation of reproductive process
cell−cell adhesion
cardiac conduction
cardiac muscle contraction
calcium ion transport
acyl−CoA metabolic process
0.4
0.5
0.6
0.7
GeneRatio
pvalue
0.01
0.02
0.03
0.04
Count
10
15
20
B
Aging and PMOS Shared
Upregulated
Downregulated
cell−substrate junction assembly
adaptive immune response
tissue remodeling
leukocyte mediated immunity
inflammatory response
mesenchymal cell differentiation
cytokine−mediated signaling
0.2
0.3
0.4
0.5
0.6
GeneRatio
pvalue
0.01
0.02
0.03
0.04
Count
10
15
20
C
PMOS Only
Upregulated
Downregulated
non−canonical Wnt signaling
hormone metabolic process
cell cycle
JAK−STAT receptor signaling
hormone biosynthetic process
extracellular matrix organization
neural precursor cell proliferation
0.30
0.35
0.40
0.45
0.50
GeneRatio
pvalue
0.005
0.010
0.015
0.020
Count
10
20
30

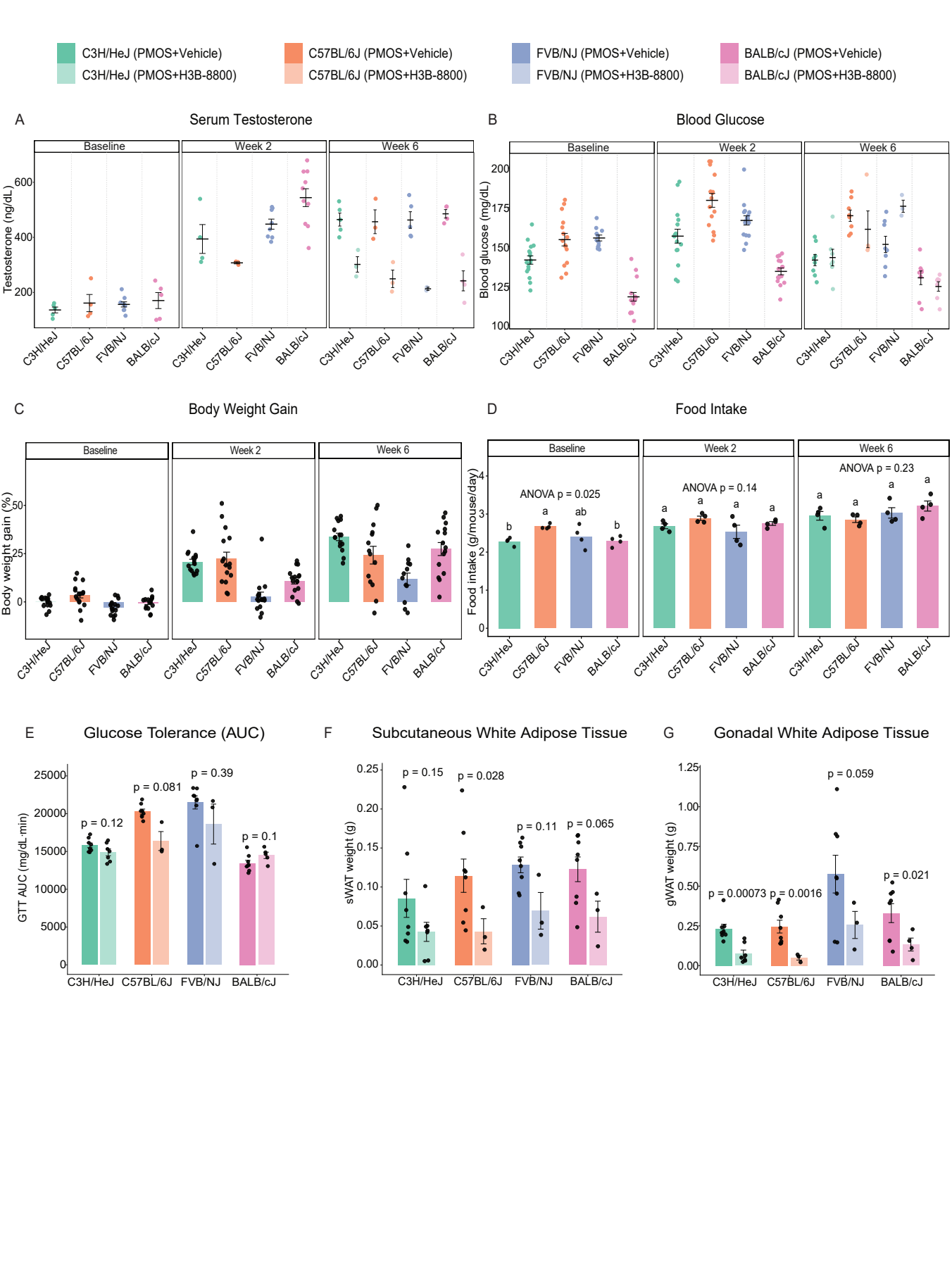
C3H/HeJ (PMOS+Vehicle)
C3H/HeJ (PMOS+H3B-8800)
C57BL/6J (PMOS+Vehicle)
C57BL/6J (PMOS+H3B-8800)
FVB/NJ (PMOS+Vehicle)
FVB/NJ (PMOS+H3B-8800)
BALB/cJ (PMOS+Vehicle)
BALB/cJ (PMOS+H3B-8800)
A
Serum Testosterone
Baseline
Week 2
Week 6
Testosterone (ng/dL)
C3H/HeJ
C57BL/6J
FVB/NJ
BALB/cJ
B
Blood Glucose
Blood glucose (mg/dL)
C
Body Weight Gain
Body weight gain (%)
D
Food Intake
Food intake (g/mouse/day)
ANOVA p = 0.025
ANOVA p = 0.14
ANOVA p = 0.23
E
Glucose Tolerance (AUC)
GTT AUC (mg/dL·min)
p = 0.12
p = 0.081
p = 0.39
p = 0.1
F
Subcutaneous White Adipose Tissue
sWAT weight (g)
p = 0.15
p = 0.028
p = 0.11
p = 0.065
G
Gonadal White Adipose Tissue
gWAT weight (g)
p = 0.00073
p = 0.0016
p = 0.059
p = 0.021

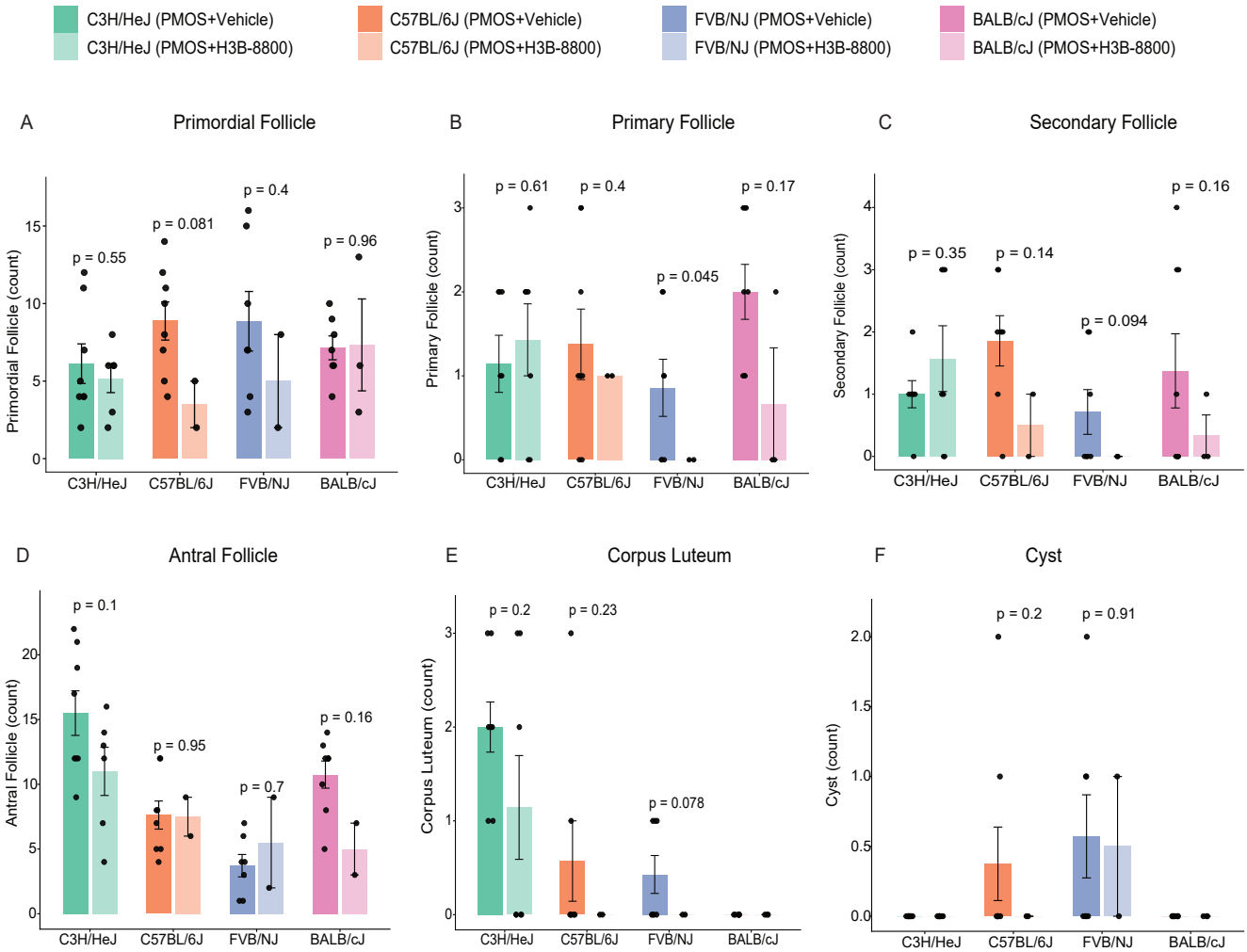
C3H/HeJ (PMOS+Vehicle)
C3H/HeJ (PMOS+H3B-8800)
C57BL/6J (PMOS+Vehicle)
C57BL/6J (PMOS+H3B-8800)
FVB/NJ (PMOS+Vehicle)
FVB/NJ (PMOS+H3B-8800)
BALB/cJ (PMOS+Vehicle)
BALB/cJ (PMOS+H3B-8800)
A
Primordial Follicle
Primordial Follicle (count)
p = 0.55
p = 0.081
p = 0.4
p = 0.96
B
Primary Follicle
Primary Follicle (count)
p = 0.61
p = 0.4
p = 0.045
p = 0.17
C
Secondary Follicle
Secondary Follicle (count)
p = 0.35
p = 0.14
p = 0.094
p = 0.16
D
Antral Follicle
Antral Follicle (count)
p = 0.1
p = 0.95
p = 0.7
p = 0.16
E
Corpus Luteum
Corpus Luteum (count)
p = 0.2
p = 0.23
p = 0.078
F
Cyst
Cyst (count)
p = 0.2
p = 0.91
C3H/HeJ
C57BL/6J
FVB/NJ
BALB/cJ

Prioritization of Drug Classes Across Cardiometabolic Traits

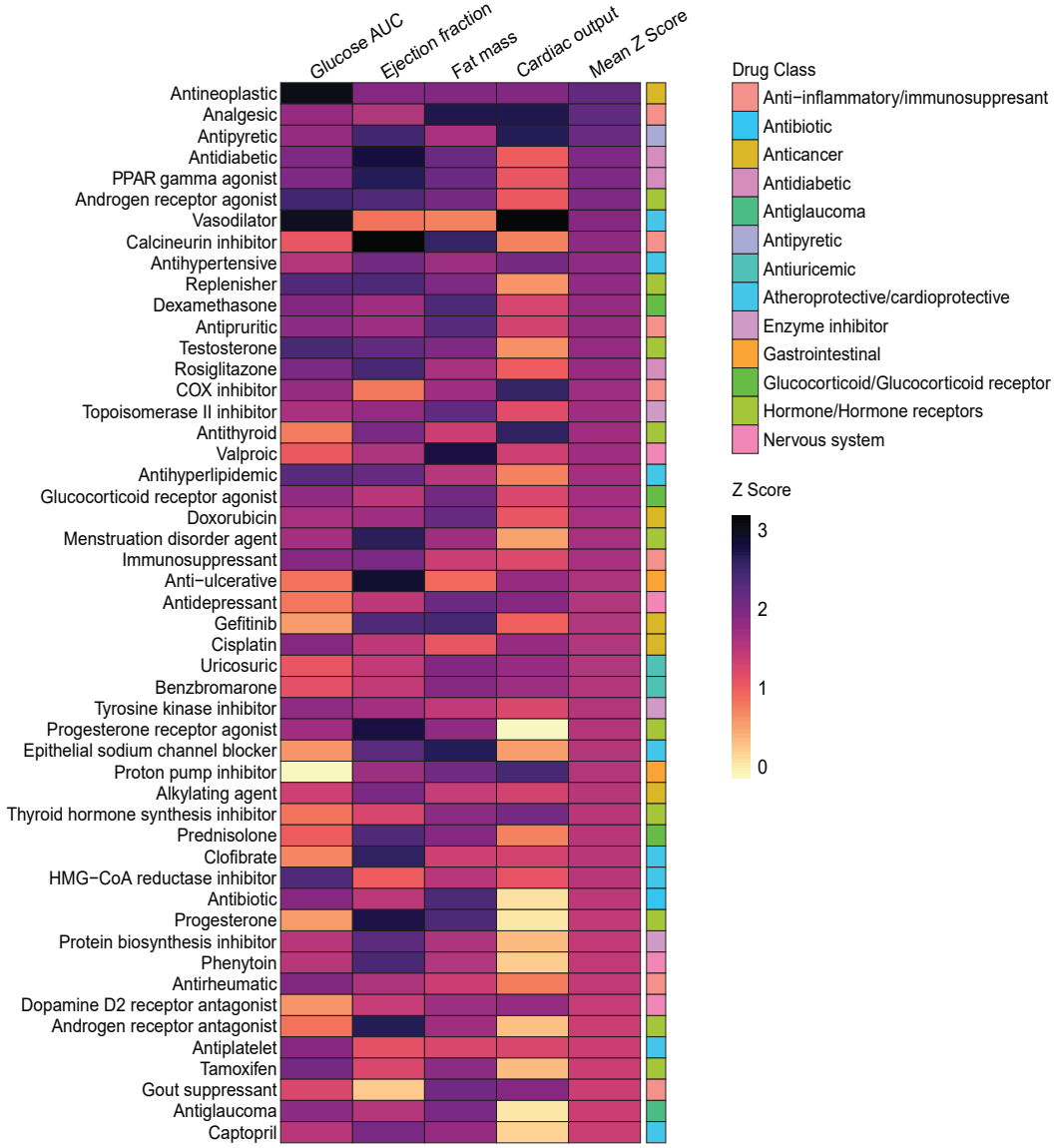

A Number of upregulated DEGs (p<0.01)

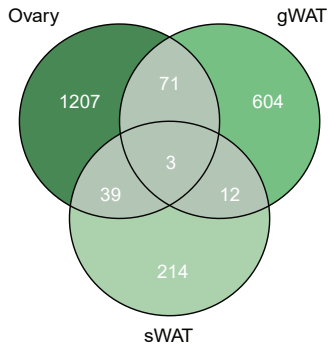

B Number of downregulated DEGs (p<0.01)

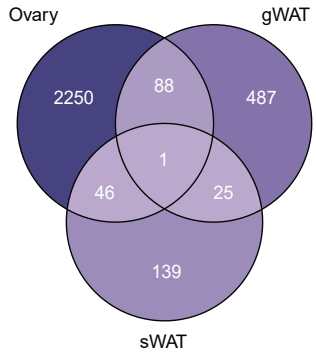

C Number of ovary genes (padj<0.05)

D Number of gWAT genes (padj<0.05)

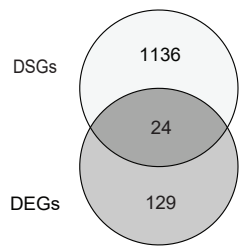

E Number of sWAT genes (padj<0.05)

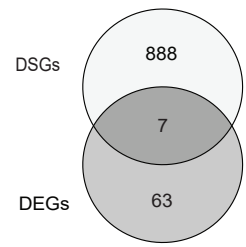

F Alternative Splicing Events in gWAT DEGs

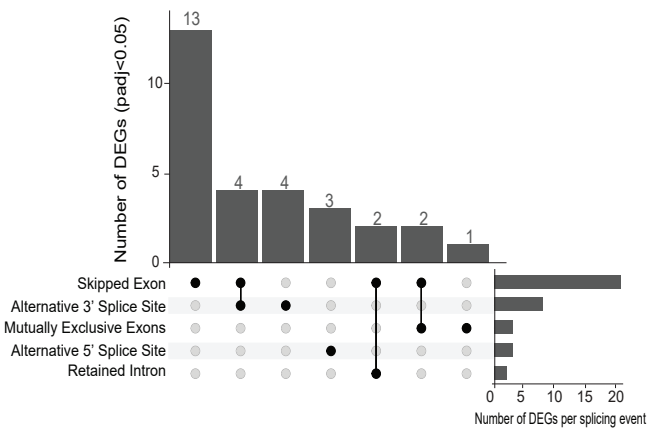

G Alternative Splicing Events in sWAT DEGs

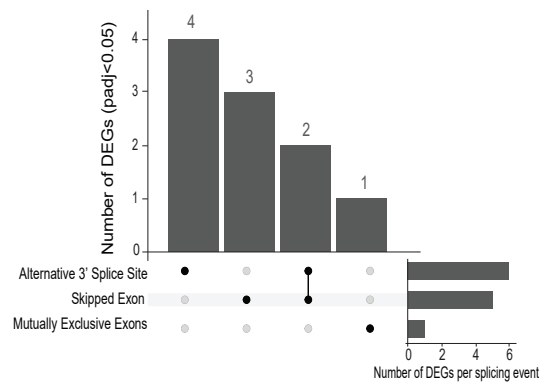

Supplemental Figure 1. Global PMOS induction of metabolic traits. A-C, Cardiac ejection fraction (A), fat mass (B), and glucose disposal rate, measured as area under the curve during glucose tolerance testing (C), in control and letrozole-induced PMOS mice. Points represent individual mice; boxes show the median and interquartile range, and whiskers extend to 1.5× the interquartile range. P values were determined by unpaired 2-tailed Student's t test.

Supplemental Figure 2. Conserved depot-specific adipose landscape of PMOS. A, Number of differentially expressed genes in ovary and adipose tissue from PMOS mice compared with control mice. Bars indicate genes suppressed or induced in each tissue. B, Top enriched pathways among adipose PMOS-associated differentially expressed genes, shown by log2 fold change in PMOS relative to control mice. Color indicates FDR. C, Intersection of differentially expressed genes between mouse PMOS gonadal adipose tissue and human PMOS subcutaneous adipose tissue or visceral adipose tissue. D, Gene Ontology overrepresentation analysis of gene sets identified from the intersections shown in C. Dot size indicates gene ratio, and color indicates adjusted P value.

Supplemental Figure 3. Integration of conserved PMOS adipose genes with single-cell and genome-wide association datasets prioritizes molecular links between PMOS, cardiovascular disease, and type 2 diabetes. A, Overlap of PMOS-associated adipose differentially expressed genes across mouse adipose tissue and human subcutaneous or visceral adipose tissue. B, Single-cell localization of core conserved PMOS adipose differentially expressed genes across female adipose cell populations. C, Colocalization of conserved PMOS adipose genes with human type 2 diabetes-associated genes. D, Gene network centered on *GNPDA2* in visceral adipose pre-adipocytes, highlighting connected pathways related to protein folding and exoribonuclease activity. E, Colocalization of conserved PMOS adipose genes with human cardiovascular disease-associated genes. F, Gene network centered on *TNS1* in mature subcutaneous adipocytes, highlighting connected pathways related to ribosomal and extracellular matrix remodeling. Gene network node size indicates gene count, and color indicates correlation coefficient.

Supplemental Figure 4. Gene set enrichment analysis of ovarian transcriptomic profiles reveals distinct and shared biological processes in PMOS and aging. A-C, Gene Ontology enrichment analysis of ovarian transcriptomic signatures showing biological processes associated with aging-specific genes (A), genes shared between aging and PMOS (B), and PMOS-specific genes (C). Terms are separated by upregulated and downregulated gene sets. Dot size indicates gene count, dot color indicates P value, and the x-axis shows gene ratio.

Supplemental Figure 5. Hormonal and metabolic phenotyping across genetically diverse PMOS mice treated with H3B-8800. A and B, Serum testosterone (A) and blood glucose (B) measured at baseline, week 2, and the vehicle/H3B-8800 comparison time point in letrozole-induced PMOS mice across C3H/HeJ, C57BL/6J, FVB/NJ, and BALB/cJ strains. Baseline and week 2 measurements were collected before H3B-8800 treatment initiation and are shown by strain to reflect responses to letrozole exposure; the final time point is shown by treatment group to compare PMOS + vehicle and PMOS + H3B-8800 mice. C, Body weight gain, calculated as percent change from baseline, across baseline, week 2, and the final treatment time point. D, Daily food intake measured across the same time points. E, Glucose tolerance test area under the curve (GTT AUC). F and G, Subcutaneous white adipose tissue (sWAT) weight (F) and gonadal white adipose tissue (gWAT) weight (G). Where treatment groups are shown, dark colors indicate PMOS + vehicle and light colors indicate PMOS + H3B-8800 within each strain: C3H/HeJ, green; C57BL/6J, orange; FVB/NJ, blue; and BALB/cJ, pink. Vehicle and H3B-8800 comparisons were performed 3 weeks after initiation of vehicle or H3B-8800 treatment, following 3 weeks of letrozole-induced PMOS induction. Points represent individual mice; bars show mean ± SEM. Sample sizes vary by assay and are indicated by individual data points, with n = 3–8 mice per strain per treatment group. For D, ANOVA P values are shown above each time point, and different letters indicate significant strain differences by post hoc multiple-

comparison testing. For E–G, P values were determined by unpaired two-tailed Student's t tests comparing vehicle and H3B-8800 treatment within each strain.

Supplemental Figure 6. Ovarian morphology across genetically diverse mouse models of PMOS treated with H3B-8800. A, Primordial follicle, B, primary follicle, C, secondary follicle, D, antral follicle, E, corpus luteum, and F, cyst counts across C3H/HeJ (green), C57BL/6J (orange), FVB/NJ (blue), and BALB/cJ (pink) mice treated with vehicle (dark color) or H3B-8800 (light color) under letrozole-induced PMOS-like conditions (n = 2-8 mice per strain per treatment group). Data are shown as mean ± SEM. Statistical comparisons were performed using unpaired two-tailed t-tests within each strain.

Supplemental Figure 7. Compound enrichment scores for PMOS trait-correlated ovarian gene networks. Z-score heatmap showing prioritization of drug classes based on network-based enrichment of drug-induced transcriptomic signatures relative to ovarian gene sets associated with PMOS-related cardiometabolic traits, including glucose area under the curve, ejection fraction, fat mass, and cardiac output. The mean Z score summarizes enrichment across traits. Drug class annotations are shown on the right. Enrichment scores were computed using the PharmOmics platform.

Supplemental Figure 8. Tissue-specific transcriptional and splicing alterations in PMOS mice treated with H3B-8800. A and B, Overlap of upregulated (A) and downregulated (B) differentially expressed genes across ovary, gonadal white adipose tissue, and subcutaneous white adipose tissue in PMOS mice treated with H3B-8800 versus vehicle. C-E, Overlap between differentially spliced genes and differentially expressed genes in ovary (C), gonadal white adipose tissue (D), and subcutaneous white adipose tissue (E). F and G, Alternative splicing event types among differentially expressed genes in gonadal white adipose tissue (F) and subcutaneous white adipose tissue (G). Bar heights indicate the number of differentially expressed genes associated with each splicing event combination, and the horizontal bars indicate the total number of genes per splicing event type. Differential expression was assessed using limma, and alternative splicing events were identified using rMATS.

Table Legends

Supplemental Table 1. Phenotypic traits measured in the mouse study. Summary of the metabolic, cardiac, hormonal, and reproductive traits measured across the genetically diverse mouse cohort for each strain.

Supplemental Table 2. Ovarian RNA-seq differential expression analysis comparing PMOS and control mice. Differential expression results from ovarian RNA-seq comparing PMOS versus control mice.

Supplemental Table 3. Marker genes used for ovarian single-cell deconvolution. Cell-type marker genes used to estimate ovarian cell-type-specific transcriptional signatures.

Supplemental Table 4. Comparison of ovarian cancer prediction models. Comparison of cancer prediction robustness between the model developed from ovarian size variation and previously published models developed to predict ovarian cancer outcomes. Study references are shown as PubMed IDs.

Supplemental Table 5. Adipose RNA-seq differential expression analysis comparing PMOS and control mice. Differential expression results from adipose tissue RNA-seq comparing PMOS versus control mice.

Supplemental Table 6. RNA-seq differential expression analysis comparing H3B-8800 and vehicle treatment. Differential expression results from ovary and adipose tissues comparing H3B-8800-treated versus vehicle-treated PMOS mice.

Supplemental Table 7. KGN cell RNA-seq differential expression analysis comparing DHT and control treatment. Differential expression results from human KGN granulosa cells comparing DHT-treated versus control conditions.